Carbon Tetrachloride as a Thermoporometry Liquid Probe To Study the Cross-Linking of Styrene Copolymer Networks

B. Husár,[†,‡] S. Commereuc,[†] I. Lukáč,[‡] Š. Chmela,[‡] J. M. Nedelec,[§] and M. Baba*[,†]

Laboratoire de Photochimie Moléculaire et Macromoléculaire, UMR CNRS 6505, Ecole Nationale Supérieure de Chimie de Clermont-Ferrand et Université Blaise Pascal, 24 Av. des Landais, 63174 Aubière Cedex, France, Polymer Institute, Centre of Excellence of Degradation of Biopolymers, Slovak Academy of Sciences, Dúbravska cesta 9, 842 36 Bratislava, Slovak Republic, and Laboratoire des Matériaux Inorganiques, UMR CNRS 6002, Ecole Nationale Supérieure de Chimie de Clermont Ferrand et Université Blaise Pascal, 24 Av. des Landais, 63174 Aubière Cedex, France

Received: October 4, 2005; In Final Form: January 16, 2006

Mesh size distributions (MSDs) of swollen cross-linked styrene copolymer networks have been measured by thermoporometry using CCl_4 as a probe liquid. All numerical relationships required for the calculation of the MSD were established for both the liquid-to-solid and the solid-to-solid thermal transitions of CCl_4 and successfully validated on test samples. It was found that the polymer network, for both thermally and photo-cross-linked materials, was completely built in about 4 h of exposure. A clear correlation was established between the average mesh size of the swollen polymer network on one hand and the benzoyl peroxide groups content and swelling ratio on the other hand.

I. Introduction

Benzil (BZ) is an industrially important member of the class of molecules with 1,2-dicarbonyl functionality. It is used in the manufacture of photographic materials and polymer resists and as photoinitiator in radical polymerizations.

The synthesis of vinyl monomers bearing benzil pendant groups and their copolymerization with styrene has been described.[1,2] It was reported that covalently attached benzil pendant groups on the polymer backbone undergo efficient peroxidation through irradiation in air at $\lambda > 400$ nm of the solid copolymer films. The conversion of α-dicarbonyl on peroxy moieties is almost quantitative. Moreover, decomposition of resulting pendant benzoyl peroxide groups (BP) offers an efficient method of effective cross-linking of polymer. The cleavage of peroxy moieties (BP) can be induced either by thermal treatment or upon irradiation at $\lambda > 300$ nm (photo-cross-linking). The photochemistry of copolymer films of these novel comonomers and styrene has been investigated. The ability of these materials to form images when irradiated through a mask has been demonstrated. In addition, these copolymers are expected to find applications in areas where controlled cross-linking is desired.

Hence, it is now necessary to characterize the final three-dimensional network in relation to the design and photoreactivity of the copolymer. Recently, the use of different techniques has been notified to reveal the network formation by cross-linking upon photooxidation of polymers. Swelling measurements,[4,5] viscosimetric analysis,[5,6] melt rheology,[7] thermoporometry,[8,9] densitometry,[10] and electron spin resonance[5] have been explored. These methods were employed for providing deeper insight on gelation phenomenon, cross-linking extent, and network structure. On the basis of previous work,[10] we decided to choose thermoporometry with CCl_4 as a liquid probe because of its ability to swell the styrene copolymer materials.

One of the obvious advantages of this technique is to monitor the network structure on a mesoscopic scale assessing information about the size of the net. We illustrate the interest of this methodology in the case of poly(1-phenyl-2-{4-[2-(4-vinylbenzyloxy)ethoxy]phenyl}ethane-1,2-dione-*co*-styrene), named poly(BZST-*co*-styrene) hereafter, shown in Scheme 1. In addition, chemical changes and network formation are easily followed by FTIR spectroscopy through the formation of ester groups as junctions units. In previous papers[1,2] very reactive monomers were used in which α-dicarbonyl was directly attached to phenyl ring of styrene unit (benzil was attached directly to the main polymer chain) or the benzil was bearing a vinyl keto polymerizing group in *para* position. On the contrary, in the present work, monomer benzil is separated from the 4-alkylstyrene group by a spacer. The reactivity of the alkyl-substituted styrenes is similar to the reactivity of the unsubstituted styrene. This fact resulted in a copolymer with much more uniform distribution of new monomer bearing benzil in the copolymer with styrene.

In this paper, some kinetic parameters of the cross-linking reaction are given and the structure of the network obtained upon irradiation is discussed in comparison with those formed by thermal treatment. Finally, an attempt is done to correlate the final three-dimensional network to peroxy moieties (BP) content during the cross-linking step.

II. Materials and Techniques

2.1. Materials. *2.1.1. Styrene Copolymer.* Synthesis of the new monomer and its copolymerization with styrene are described in ref 3. Poly(BZST-*co*-styrene) contains 2.6 wt %

* To whom correspondence should be addressed. E-mail: mohamed.baba@univ-bpclermont.fr.

† UMR CNRS 6505, Ecole Nationale Supérieure de Chimie de Clermont-Ferrand et Université Blaise Pascal.

‡ Centre of Excellence of Degradation of Biopolymers, Slovak Academy of Sciences.

§ UMR CNRS 6002, Ecole Nationale Supérieure de Chimie de Clermont Ferrand et Université Blaise Pascal.

10.1021/jp055648i CCC: $33.50
Published on Web 02/22/2006

SCHEME 1: Photoreactivity of Poly(1-phenyl-2-{4-[2-(4-vinylbenzyloxy)ethoxy]phenyl}ethane-1,2-dione-*co*-styrene)

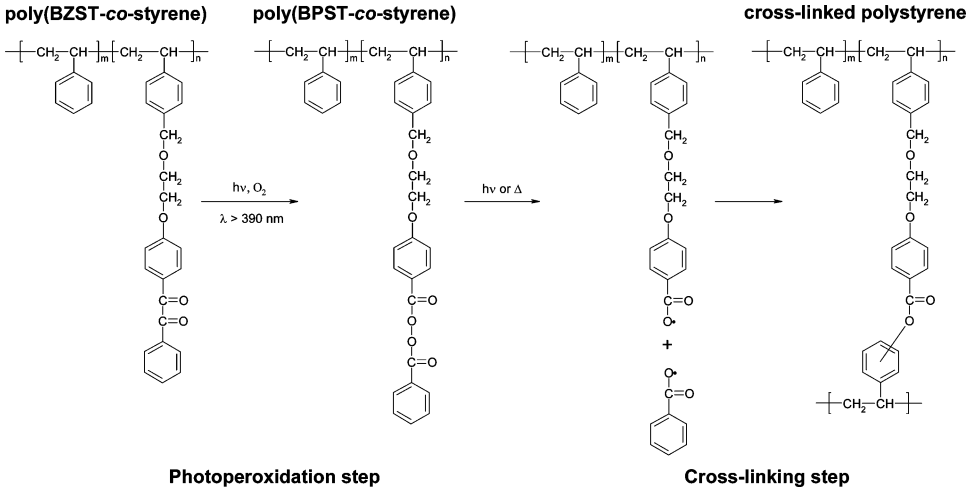

TABLE 1: Textural Data for the Nanoporous Calibration Samples

sample	SSA ($m^2 \cdot g^{-1}$)	V_p ($cm^3 \cdot g^{-1}$)	R_p (nm)
1	472.7	0.922	3.42
2	166.2	0.991	8.7
3	183.1	1.327	14.25
4	111.6	0.680	7.5
5	406.9	0.813	3.1

of benzil pendant groups on the basis of NMR determination. Molecular weights were determined by SEC measurements using a polystyrene calibration (M_n= 200 000, M_w= 450 000). Films were prepared by compression molding between two Teflon sheets during 1 min at 150 °C under 190 bar. The thickness of the films was about 100 μm.

2.1.2. Porous Samples. Nanoporous silica gels monoliths with tailored texture[1−3] were prepared as described elsewhere.[11] Additional commercial porous glass beads[4] were also used as reference material for the calibration procedure.

Commercial silica gel for chromatography[5] was used as a test sample to confirm the validity of the calibration procedure. The textural properties of the different materials have been measured by nitrogen gas sorption technique (BJH method) on a Quantachrome Autosorb6 apparatus, and results are given in Table 1. Nanoporous sol−gel derived silica samples are particularly valuable since their monolithic form allows easy handling.

CCl_4 (Aldrich) of HPLC quality was used without any supplementary purification.

2.2. Analysis. A Mettler-Toledo DSC 30 apparatus was used to carry out the thermal analysis. It was equipped with a liquid nitrogen cooling unit permitting to scan temperatures ranging from −170 to 500 °C. A cooling/heating rate 0.7 °C·min^{-1} was adopted. This rate value has been determined to be slow enough to keep the system under a continuous thermodynamically equilibrium state.

Calibration, in terms of temperature and heat, was performed using *n*-heptane (−90.6 °C, 140.5 J·g^{-1}), indium (156.6 °C, 28.45 J·g^{-1}), and zinc (419.2 °C, 107.5 J·g^{-1}) as references. A dedicated software allows various calculations (onset, heat, peak temperature, etc.) from the original recorded DSC curves.

An Impact 400 FTIR spectrophotometer, supplied by Nicolet Co. (Omnic software), was used to record the FTIR absorption spectra of the copolymer films after various photooxidation and curing times of the cross-linking process.

2.3. Cross-Linking Procedure. Irradiations were performed using a polychromatic light from SEPAP device (ATLAS Corp.) which has been described in ref 12.

An aerated oven was used for the heating experiments.

III. Results and Discussion

3.1. Thermoporometry Experiments. The theoretical basis of this technique was already largely reported,[13−15] and it is admitted now that the thermoporometry (or thermoporosimetry) is a good tool to study divided medium. The technique relies on the experimental evidence that confined liquid, within a pore or "compartimentized" in a gel, freezes at a temperature lower than the one of bulk liquid. The shift of the transition temperature is related to the size of the confinement volume. Particularly, thermoporometry is a suitable method to study the soft and fragile materials provided that a proper liquid probe is chosen. Indeed, Scherer and co-workers[16,17] reported that a shrinkage can occur when the swelling liquid crystallizes. In the case of water for instance, and because of the higher molar volume of ice compared to liquid water, crystallization can provoke damage within the gel network.

We have chosen CCl_4 as liquid probe to explore the cross-linking of styrene copolymer materials. CCl_4 is a good solvent of non-cross-linked polystyrene; its thermal transition temperatures are not too low, and it is available at high purity grade. Furthermore, the solid CCl_4 being denser than its liquid form, and no important shrinkage is expected when the confined solvent crystallizes. Anyway, even if the swollen gel undergoes dimensional variations because of the thermal transition of the liquid probe, these variations must be small compared to the ones induced by swelling. Thermoporometry consequently remains an efficient and unique tool to compare the state of cross-linking of different polymeric samples. The mesh size distributions calculated from the thermoporometry formalism reflect the actual state of the sample taking in account the eventual shrinkage and the swelling equilibrium.

Bulk CCl_4 was studied before, and its thermal phase transitions were well characterized.[18,19] It exhibits a complex thermal transitions system as shown in Figure 1.

Takei et al.[19] showed that both solid-to-solid and liquid-to-solid transitions of CCl_4 were strongly dependent on the average pore size of the porous medium in which the liquid is confined. In particular, they demonstrated that the liquid-to-I_a transition disappears when the pore radius is smaller than 16.5 nm that is the case of all our calibration samples (see Table 1).

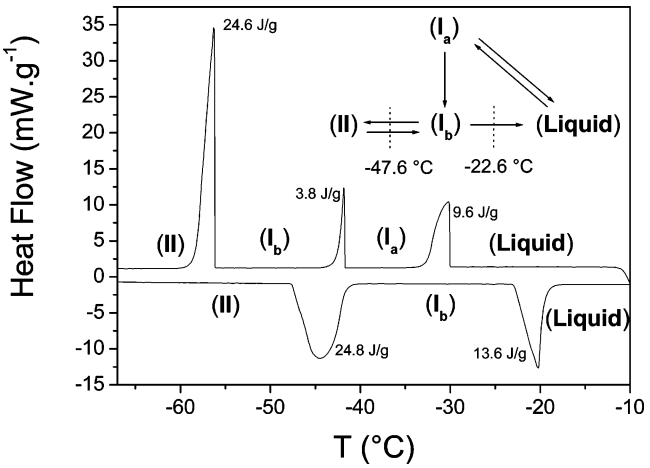

Figure 1. DSC thermogram showing the complex thermal transition system of bulk CCl_4. The scanning rate was 0.7 °C·min^{-1}.

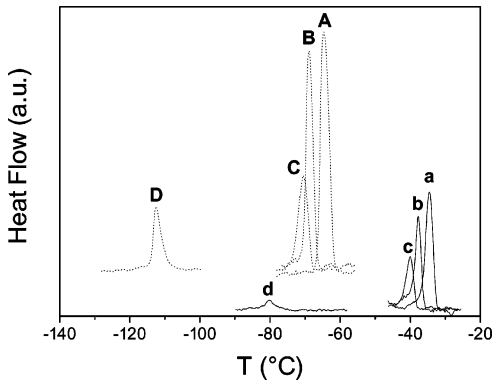

Figure 2. DSC thermograms of confined CCl_4 within the calibration samples: (a, A) sample with 14.25 nm as pore radius; (b, B) 8.7 nm; (c, C) 7.5 nm; (d, D) 3.42 nm. Solid lines represent the liquid-to-I_b and the dashed lines the I_b-to-II thermal transitions. The cooling rate was 0.7 °C·min^{-1}.

3.1.1. Calibration Procedure. A direct calibration procedure using the silica gel samples having well-defined textural properties has been already described.[14,19,20] We applied the same procedure to establish the empirical relationships linking the pore radius (R_p) and the shift of transition temperature of the confined CCl_4 (ΔT).

Figure 2 shows the DSC thermograms related to the cooling of CCl_4 confined in the calibration samples. For each calibration sample, two peaks are observed: a−d correspond to the liquid-to-I_b crystallizations; A−D are attributed to the corresponding I_b-to-II allotropic transitions. As expected, the smaller the pore radius, the lower the temperature at which the confined liquid undergoes the transition. The similar behavior is observed for the two transitions. On the other hand, the area under peak, which is proportional to the released energy, decreases with respect to the pore radius.

Figure 3 shows the graphic representations of pore radius (R_p) versus the transition point depression, $\Delta T = T_p - T_0$, related to the liquid-to-I_b and the I_b-to-II transformations. T_0 is the bulk CCl_4 melting temperature (corresponding to the onset point of the fusion endotherm for liquid-to-solid transition), and T_p is the temperature of the phase transition inside the pore (taken at the top of the peak as recommended by Landry).[21] In the same figure, the data published earlier by Brun and co-workers[18] were also plotted. A good agreement can be seen between the two series.

No linear dependence was observed between the pore radius (R_p) and the reciprocal shift of transition temperature (ΔT^{-1}).

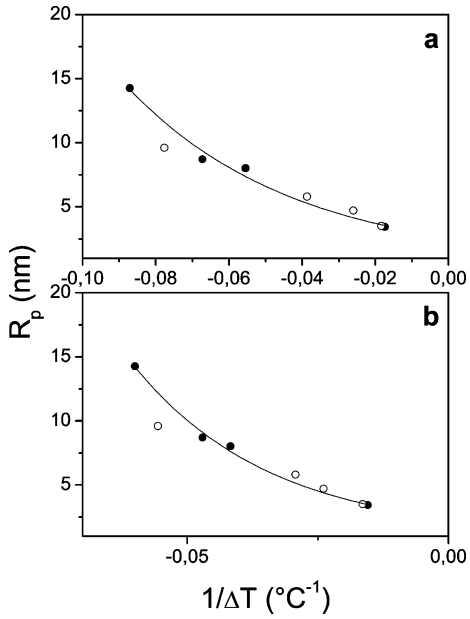

Figure 3. Dependence of pore radius against the depression transition point: (a) liquid-to-solid transition; (b) solid-to-solid transition. The opened symbols represent the data published by Brun and co-workers.[18]

TABLE 2: Numerical Parameter Values of the Relationships between the Apparent Energy of Thermal Transitions (W_a) and Their Depression Temperature (ΔT) and between the Pore Radii (R_p) and ΔT^{-1}

	$R_p = t\exp(-b/\Delta T)$		$W_a = W_0\exp(f\Delta T)$	
transitn	t (nm)	b (°C)	W_0 (J·cm^{-3})	f (°C^{-1})
liquid-to-solid	2.43	20.1	25.07	0.04
solid-to-solid	2.09	31.6	46.6	0.017

The same kind of relationship was already observed for several others thermoporosimetry liquid probes.[9,22−24] This observed nonlinearity could be related to the strong temperature dependence of the latent enthalpy of transition (W_a). The apparent enthalpies of both liquid-to-solid and solid-to-solid transition have been calculated by following the same procedure described elsewhere.[22] Table 2 summarizes the expressions of R_p and W_a as function of ΔT.

3.1.2. Control of the Calibration. To check the pertinence of the calibration empiric relationships, PSDs of two samples were calculated using the obtained numerical equations. The first one is a commercial silica gel powder used for column chromatography with 6.0 nm nominal pore diameter. The second control sample is a powdered porous glass, the textural properties of which can be found in Table 1. This sample being used for the calibration, the mean pore size is obviously well reproduced, but it is striking to note that the whole pore size distribution is indeed very well reproduced by thermoporometry using both transitions. Figure 4 gives a comparison between PSDs calculated from the gas adsorption technique with the BJH model and the thermoporometry experiments. The two series of data seem in good agreement, thus validating our calibration procedure. Figure 4b shows a certain discrepancy between the nitrogen gas sorption and thermoporometry results in the lowest R_p side. This observation may be explained by the R_p expression given in Table 2. The t value, 2.09 nm for the solid-to-solid transition, represents the lowest R_p which can be measured by thermoporometry method and which is reached when ΔT tends toward infinity.

3.2. Application to Styrene Copolymer Networks. *3.2.1. Evolutions of the Mesh Sizes Distributions.* The poly(BZST-

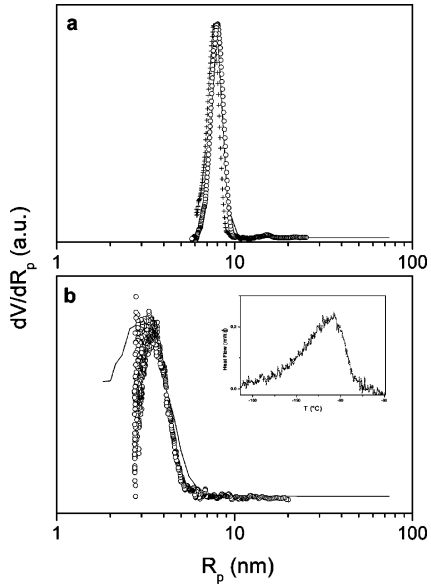

Figure 4. Pore size distributions derived from gas (N_2) adsorption (lines) and from thermoporosimetry technique (symbols) for glassy beads with 7.5 nm of average pore radius (a) and for column chromatography silica gel (b). The inset figure shows the DSC thermogram of the solid-to-solid transition of CCl_4 within silica gel powder. ○ represents the PSD calculated from the solid-to-solid transition, and +, the PSD calculated from the liquid-to-solid one in (b). Because of the weak intensity of the liquid-to-solid peak, only the solid-to-solid transition was used.

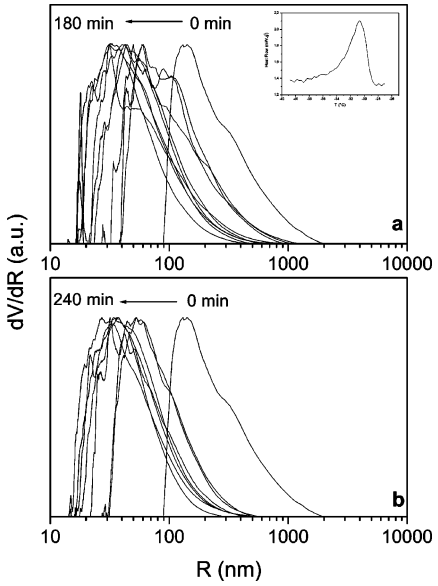

Figure 5. Mesh sizes distributions of the polymer networks of cross-linked poly(BZST-*co*-styrene) samples. The films were at first irradiated in air at $\lambda > 390$ nm at 35 °C to transform the benzil pendant functions (BZ) into benzoyl peroxide groups (BP) and after then either thermally cross-linked at 110 °C (a) or photo-cross-linked by irradiation at $\lambda > 300$ nm at 35 °C (b). The inset figure shows an example of a DSC thermogram of the liquid-to-solid transition of CCl_4 swelling a thermally cross-linked copolymer sample.

co-styrene) films, peroxidized at $\lambda > 390$ nm and then cross-linked by heating at 110 °C or by irradiation at $\lambda > 300$ nm, were swollen in CCl_4 for 48 h. A 10−20 mg amount of the swollen gel was taken and set in the DSC crucible. The temperature program, described in the calibration section, was applied to record the DSC thermograms of the CCl_4 confined inside the polymer gel. As it was assumed in several previous papers,[9,22,25] a formal analogy exists between the notion of the pore in the rigid porous material and that of the mesh in the swollen polymeric gel. CCl_4, swelling the soft material, is confined, and its degrees of freedom are reduced in the same way as when it is trapped inside the porous material. Even if there are no pores in the polymer gel, the mobility of the liquid is limited in the two cases. Mesh sizes distributions, calculated for various photo-cross-linked and thermally cross-linked poly-(BZST-*co*-styrene) samples, are presented in Figure 5. The exposure or the cure time increases from right to left. The inset, in Figure 5a, shows a typical DSC thermogram of CCl_4 confined in the swollen gel. Only the liquid-to-solid thermal transition of CCl_4 was used. At first glance, one can notice that the MSD globally shifts toward smaller values of mesh sizes (from 370 to 60 nm) when the time increases. This behavior reveals a densification of the polymer network corresponding to an increase of the cross-linking level. It is also noticeable that no significant variation of the MSD was detected after 4 h regardless of the cross-linking conditions. Both irradiation and heating treatment seems to have the same effect on the polymer matrix.

3.2.2. Correlation between the Thermoporometry and the Results from FTIR Measurements. According to the mechanism depicted in Scheme 1, the cross-linking is due to the cleavage of the benzoyl peroxide functions and the subsequent ester groups formation. Conversion of benzil pendant groups (BZ) during the photoperoxidation step (irradiation at $\lambda > 300$ nm at 35 °C) was easily followed by FTIR spectroscopy. As the reaction proceeds, the intensity of the characteristic FTIR

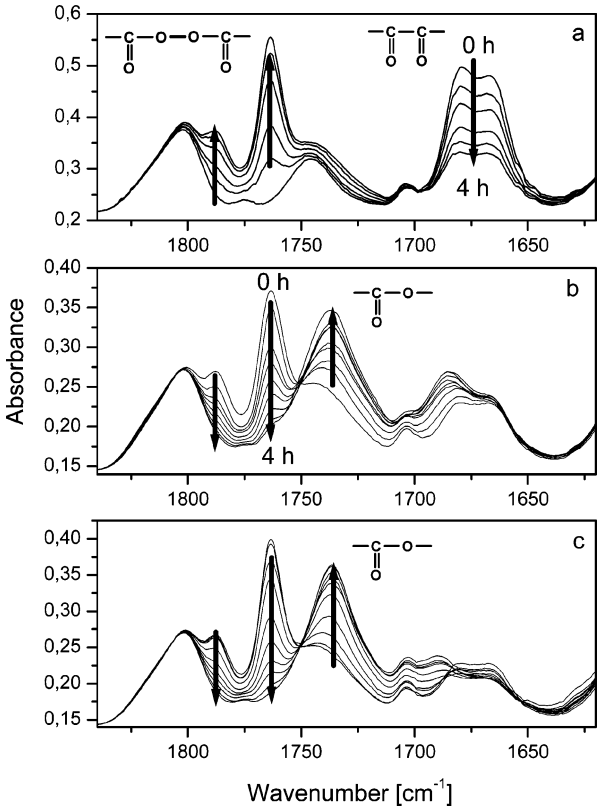

Figure 6. FTIR spectra of poly(VBZ-*co*-styrene) films. Peroxidation step: films were irradiated at $\lambda > 390$ nm at 35 °C in air (a). Cross-linking step by thermal treatment: peroxidized films were heated at 110 °C in an aerated oven (b). Photo-cross-linking step: peroxidized films were irradiated at $\lambda > 300$ nm at 35 °C in air (c). The periods of each treatment ranged between 0 and 240 min.

stretching band of 1,2-dicarbonyl groups at 1675 cm^{-1} decreases (see Figure 6a). Formation of BP moieties is detected in FTIR

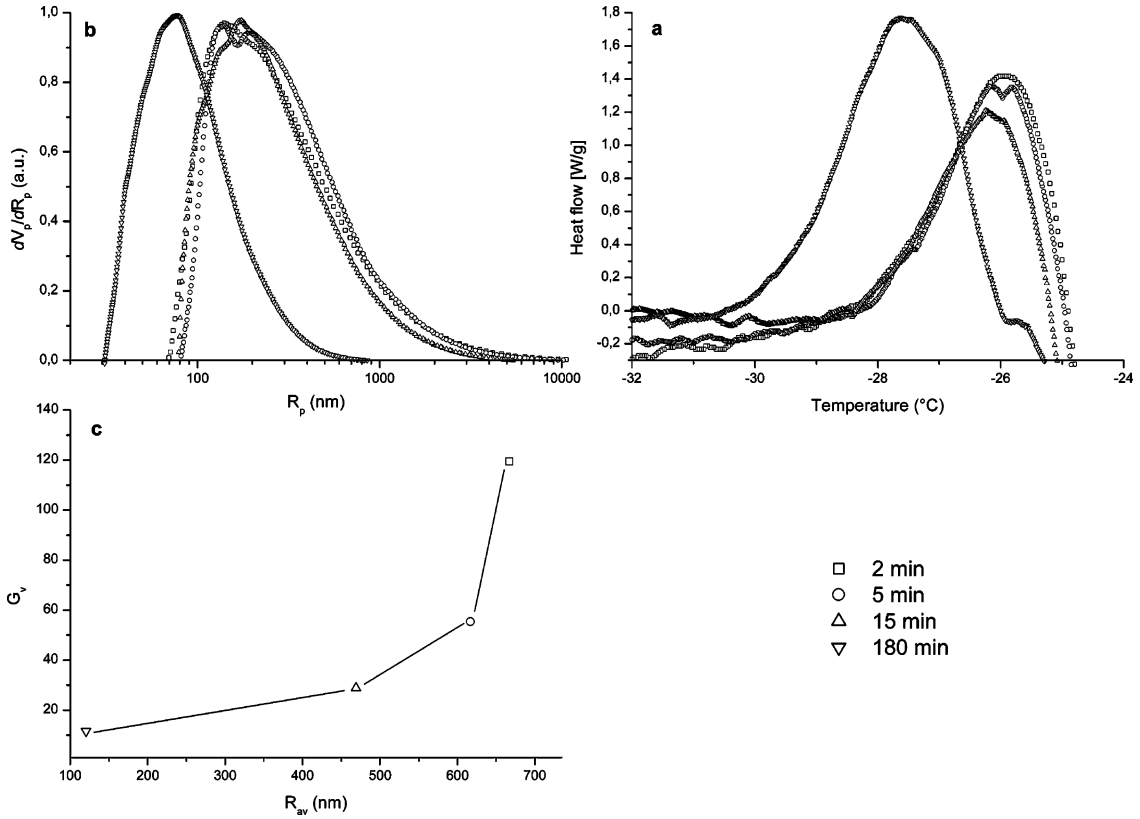

Figure 7. Correlation between the average mesh size of the network (R_{av}) and the degree of swelling (G_v): (a) DSC exotherms of solidification of the confined CCl_4 for four irradiated and swollen samples (□, 2 min; ○, 5 min; △, 15 min; ▽, 180 min); (b) corresponding mesh size distributions; (c) plot of the degree of swelling measured by the gravimetric method (G_v) versus the average mesh size (R_{av}) derived from thermoporometry.

spectra by the growth of new absorption bands at 1765 and 1785 cm^{-1} ascribed to benzoyl peroxide groups.

The cross-linking step leads to significant changes in the IR absorption spectra. Figure 6 displays the chemical evolution of peroxidized sample poly(BPST-*co*-styrene) upon either thermal cross-linking at 110 °C either photo-cross-linking at $\lambda > 300$ nm at 35 °C.

The thermal decomposition of BP groups is detected by the decrease of the peroxide absorption bands in the region 1750−1800 cm^{-1} and the increase of an absorption band at 1740 cm^{-1} assigned to the ester links formation. The thermal decomposition of photochemically generated BP groups in poly(BZST-*co*-styrene) film is achieved upon 4 h of treatment at 110 °C.

Similar results are obtained through the photo-cross-linking process. Figure 6c monitors the phototransformation of BP groups (absorbing in the region 1750−1800 cm^{-1}) into ester bridges (at 1740 cm^{-1}) linking the macromolecular chains to each other. After 4 h of UV exposure at $\lambda > 300$ nm, the peroxide moiety is no longer detected in the FTIR spectrum.

To correlate the disappearance of benzoyl peroxide (BP) and the morphological evolution of the polymer matrix, the average size (R_{av}) of the mesh of the network was calculated from each MSD. Our assumption is that the average size of the mesh is related to the degree of swelling and can be used as cross-linking indicator: the smaller R_{av}, the denser the polymeric network. To confirm this assumption, prior to use of the R_{av} data, some experiments have been performed to compare the thermoporometry results with gravimetric swelling measurement, which is the more conventional method to characterize the three-dimensional network. For four new samples, irradiated respectively for 2, 5, 15, and 180 min, the degrees of swelling (G_v) were determined by the gravimetric method. The same samples were then submitted to the thermoporometry procedure, and their average mesh size was been calculated. Figure 7 summarizes the results of these experiments. As can be seen in Figure 7c, it can be pointed out that R_{av} increases with the degree of swelling, thus confirming our working hypothesis.

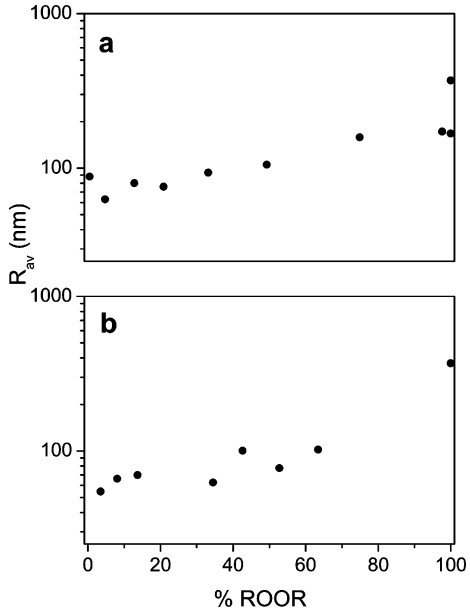

Figure 8. Correlation between the relative homolyzed benzoyl peroxide concentration (% ROOR) and the average mesh size (R_{av}) of the polymer network during irradiation at $\lambda > 300$ nm at 35 °C (a) and heating at 110 °C in air (b). The films were at first peroxidized at $\lambda > 390$ nm at 35 °C in air.

Figure 8 presents the evolution of R_{av} with respect to the relative homolyzed benzoyl peroxide concentration (% ROOR).

The % ROOR was determined on the basis of IR analysis by rationing absorbances at 1765 cm^{-1} as follows:

$$\% \text{ ROOR} = \frac{A(t)}{A_0} \times 100$$

Here $A(t)$ is the absorbance at 1765 cm^{-1} for a given exposure time (t) and A_0 the initial absorbance.

Regardless of the cross-linking conditions (heating or irradiation), an actual correlation can be observed between the cleavaged peroxide content of the matrix and the average mesh size of the network. The origin of cross-linking is then clearly established. Thus, we assume that while peroxide cleavage is clearly responsible for cross-linking, the BP content defines the structure of the final network. Besides, Figure 8a exhibits two distinct values of R_{av} corresponding apparently to an identical percentage of ROOR (100%). A possible explanation of this observation may be the better sensitivity of the thermoporometry by comparison with the IR spectroscopy. In fact, a small diminution in % ROOR, not detectable by IR investigation, can cause a noticeable morphological modification in the polymeric network which may be measurable by thermoporometry.

Conclusion

Films of poly(BZST-*co*-styrene) were irradiated at $\lambda > 390$ nm to transform pendant benzil dicarbonyl groups (BZ) into pendant benzoyl peroxide groups (BP). The pendant benzoyl peroxide groups were converted, either by irradiation at $\lambda > 300$ nm or heating at 110 °C, into ester functions linking the macromolecular chains to each other and leading to a cross-linked material. This chemical evolution is conventionally monitored by FTIR spectroscopy or gravimetric swelling method. Thermoporometry, giving the mesh size distribution of the polymer network for different irradiation or curing times, is an alternative and complementary way to follow these alterations. A pertinent correlation between these three approaches was clearly established.

CCl_4, as thermoporometry liquid probe, seems to be very suitable to study the cross-linking of the styrene copolymers. All the numerical relationships, needed to perform the calculation of the mesh sizes distributions from DSC thermograms, were established, and their validity was successfully checked for the two thermal transitions of CCl_4.

Acknowledgment. The authors are grateful to the VEGA agency for financial support through Grant 2/5108/25. Financial support from the French ANR under project Nanothermomécanique (ACI Nanosciences No. 108) is gratefully acknowledged.

References and Notes

(1) Mosnáček, J.; Weiss, R. G; Lukáč, I. *Macromolecules* **2002**, *35*, 3870.
(2) Mosnáèek, J.; Weiss, R. G.; Lukáč, I. *Macromolecules* **2004**, *37*, 1304.
(3) Husár, B.; Lukáč, I. *Polym. Photochem. Photobiol., A: Chem.* Submitted for publication.
(4) Giurginca, M.; Zaharescu, T. *Polym. Degrad. Stab.* **2002**, *75*, 267.
(5) Chipara, M. I.; Georgescu, L.; Oproiu, C.; Chipara, M. D.; Niculescu, A.; Galatanu, N.; Reyes, J. R.; Secu, C. E. *NIM Phys. Res.* **1997**, *B131*, 188.
(6) Adam, C.; Lacoste, J.; Lemaire, J. *Polym. Degrad. Stab.* **1991**, *32*, 51.
(7) Commereuc, S.; Bonhomme, S.; Verney, V.; Lacoste, J. *Polymer* **2000**, *41*, 917.
(8) Baba, M.; Gardette, J. L.; Lacoste, J. *Polym. Degrad. Stab*. **1999**, *63*, 121.
(9) Baba, M.; Nedelec, J. M.; Lacoste, J.; Gardette, J. L. *J. Non-Cryst Solids* **2003**, *315* (3), 228.
(10) Baba, M.; Gardette, J. L.; Lacoste, J. *Polym. Degrad. Stab*. **1999**, *65*, 421.
(11) Hench, L. L. In *Sol−gel silica: processing, properties and technology transfer*; Noyes Publications: New York, 1998.
(12) Lemaire, J.; Arnaud, R.; Gardette, J. L.; Lacoste, J.; Seinera. *Kunstst.*—Ger. Plast. **1986**, *76*, 149.
(13) Kunh, W. Peterli, E.; Majer, H. *J. Polym. Sci*. **1955**, *16*, 539−548.
(14) Brun, M.; Lallemand, A.; Quinson, J. F.; Eyraud, C. *Thermochim. Acta* **1977**, *21*, 59.
(15) Rudman, R.; Post, B. *Science* **1966**, *154*, 1009.
(16) Scherer, G. W. *J. Non-Cryst. Solids* **1993**, *155*, 1−25.
(17) Scherer, G. W.; Smith, D. M.; Stein, D. *J. Non-Cryst. Solids* **1995**, *186*, 309−315.
(18) Brun, M.; Quinson, J. F.; Martinie, B.; Eyraud, C. *J. Chim. Phys.* **1978**, *75*, 469−475.
(19) Takei, T.; Ooda, Y.; Fuji, M.; Watanabe, T.; Chikazawa, M. *Thermochim. Acta* **2000**, *352−353*, 199−204.
(20) Denoyel, R.; Pellenq, R. J. *Langmuir* **2002**, *18*, 2710.
(21) Landry, R. *Thermochim. Acta* **2005**, *433*, 27−50.
(22) Billamboz, N.; Nedelec, J.-M.; Grivet, M.; Baba, M. *ChemPhysChem* **2005**, *6*, 1−7.
(23) Billamboz, N.; Baba, M.; Grivet, M.; Nedelec, J. M. *J. Phys. Chem. B* **2004**, *108*, 12032−12037.
(24) Bahloul, N.; Baba, M.; Nedelec, J. M. *J. Phys. Chem. B* **2005**, *109*, 16227−16229.
(25) Baba, M.; Nedelec, J. M.; Lacoste, J.; Gardette, J. L.; Morel, M. *Polym. Degrad. Stab.* **2003**, *2*, 80.